Research Article | Vol. 27, No. 4 | 18 Feb 2019 | OPTICS EXPRESS 5557
Optics EXPRESS

Comparative study of NIR-MIR beamsplitters based on ZnS/YbF_3 and Ge/YbF_3

TATIANA AMOTCHKINA,[1] MICHAEL TRUBETSKOV,[2] MARCUS SCHULZ,[3] AND VLADIMIR PERVAK[1,*]

[1]*Ludwig-Maximilians-Universität München, Am Coulombwall 1 85748, Garching, Germany*
[2]*Max-Planck-Institut für Quantenoptik, Hans-Kopfermann-Str. 1 85748, Garching, Germany*
[3]*Agilent Technologies, Hewlett-Packard-Str. 8, 76337 Waldbronn, Germany*
[*]*Vladimir.Pervak@lmu.de*

Abstract: Two beamsplitters operating across the near-infrared (770-1050 nm) and mid-infrared (4-8 µm) spectral ranges are developed. For the first time, the beamsplitters based on thin-film materials combinations of ZnS/YbF_3 and Ge/YbF_3 are investigated. The multilayers operate at the Brewster angle of ZnSe substrate. There are no special temperature conditions. The dichroic coatings are designed, produced, and carefully characterized. Potentials of the ZnS/YbF_3 and Ge/YbF_3 thin-film material combinations are discussed based on analytical estimations, as well as on optical and non-optical characterization results. The ZnS/YbF_3 pair provides high reflectance in the near-infrared spectral range. The Ge/YbF_3 solutions exhibit very broadband reflection zones. The Ge/YbF_3 coatings are thinner and comprise fewer layers than ZnS/YbF_3 multilayers. Ge/YbF_3 pair has high potential for design and production of NIR-MIR coatings.

1. Introduction

In the recent years, the mid-infrared (MIR) spectral range from 3 to 15 µm attracts more and more interest of chemists and biologists since most organic molecules exhibit fundamental vibrational and rotational modes in this range [1,2]. Several research groups investigate organic compounds in the gaseous or liquid phase with the help of powerful laser systems (see, for example [3,4],). Harnessing MIR radiation in the laser systems demands high quality multilayer optical elements operating in the near-infrared (NIR) *and* in the MIR spectral ranges, so called *NIR-MIR coatings*. Typically, such coatings are used to split or combine the laser beams into more powerful near-infrared and less powerful mid-infrared components. The coatings exhibit desired reflectance in a specified NIR range and high transmittance in a required MIR region. The acceptable levels of reflectance and transmittance as well as the angle of incidence (AOI) are dependent on the laser setup and the goals of the laser experiments. In addition, target specifications arising from the application area may contain not only desired *spectral* performance but also *non-optical properties* (good adhesion, low mechanical stress, thermal stability). For laser applications, the low mechanical stress is crucial in order not to deform the laser beam wave front of the entire laser system. These specifications affects the choice of thin-film materials and design structures since the coatings operating in the MIR range may contain thick layers, and adhesion or/and stress problems may arise at some combinations of substrate/thin-film materials.

In the present work, two NIR-MIR beamsplitters (BS) on ZnSe substrates with sophisticated target spectral characteristics are reported. The multilayer elements operate at the Brewster angle of the ZnSe substrate (67.9°). The beamsplitters are supposed to exhibit reflectance (p-polarized light) exceeding 75% in the range from 860 to 1050 nm, high reflectance (s-polarized light) exceeding 95% in the range from 770 to 830 nm, and high transmittance close to 100% in the MIR range from 4 to 8 µm. The reflectance curves in the high reflection (HR) zones should cover the entire spectral range of interest, i.e., they have to exhibit minimal deviations from the average reflectance value for both polarizations. The optical elements should exhibit low mechanical stress. The beamsplitters can be used in

#355772 https://doi.org/10.1364/OE.27.005573
Journal © 2019 Received 20 Dec 2018; revised 30 Jan 2019; accepted 30 Jan 2019; published 13 Feb 2019

Optics EXPRESS

pump-probe spectroscopy studying ultrashort dynamics of biological molecules. Three possible pairs of three thin-film available materials, namely ZnS, Ge, and YbF_3, were used for design of the BS. Two BS comprising ZnS/YbF_3 and Ge/YbF_3 layers were successfully produced using e-beam evaporation. After the deposition, beamsplitters were optically characterized and their adhesion was tested with the help of a tape. Mechanical stresses of the designs were estimated based on stresses in single films of Ge, YbF3, and ZnS using a well-known formula [5,6]. Although Ge layers are absorbing in the HR zones, Ge/YbF_3 multilayers demonstrate a few benefits in comparison with the non-absorbing pair ZnS/YbF_3, namely, very broadband high-reflection zones, smaller number of layers and smaller total thickness. Optical and non-optical properties of the manufactured multilayer elements were compared. The third pair Ge/ZnS did not provide the desired reflectance values already at the design step.

According to our knowledge, the thin-film materials combinations ZnS/YbF_3 and Ge/YbF_3 have been exploited for the production of a sophisticated NIR-MIR multilayer beamsplitters for the first time. There exist only several publications reporting on production of *single* YbF_3 thin films (see, for example [7–9],). The YbF_3 thin-film material was chosen based on its optical and mechanical properties reported in the literature sources [10–13]. Having a low refractive index ≈ 1.5, YbF_3 replaces highly toxic ThF_4 which was used earlier as a low-index material in MIR coatings [14]. Also, the refractive index contrast of YbF_3 with Ge is very high (≈ 2.7, and with ZnS is relatively high (≈ 1.5). YbF_3 is highly suitable for e-beam evaporation [11–13]. YbF_3 films are transparent from 200 nm up to 12 um [11,12,15], they exhibit low tensile stress lower than at a number of other fluoride materials [11], and good environmental resistance [11,13]. In addition to this, the deposition/characterization experience with YbF_3 was already accumulated. This experience was in a full agreement with reference data [10–13].

2. Design approach

The NIR-MIR beamsplitters were produced using Syruspro710 deposition plant (Bühler Leybold Optics, Germany) based on the electron-beam evaporation. The nominal refractive indices of Ge, ZnS, and YbF_3 thin films in the broadband spectral range from 400 nm to 8000 nm were accurately determined based on optical characterization of single-layer samples and test multilayers containing a small number of layers. The ZnSe substrate was optically characterized in the range 400-8000 nm. Optical constants of Ge thin layers were found using a non-parametric approach [16,17] that allows one to solve the most complicated characterization problems, where the optical constants cannot be described by well-known few-parametric models such as Cauchy or Sellmeier. Also, this approach is applied when optical constants in a very broad spectral range are to be determined. Refractive indices of YbF_3, ZnS, and ZnSe were determined using Cauchy model and cross-checked using the non-parametric approach. The detailed description of the sophisticated characterization process of the MIR films in a broadband spectral range lies out of the scope of the current manuscript and will be published separately. In Fig. 1(a), the nominal refractive indices of ZnS, Ge, YbF_3 layers, and ZnSe substrate are plotted; Fig. 1(b) shows the extinction coefficients of Ge layers and ZnSe substrate.

Design of the BS was performed by the needle optimization algorithm incorporated into OptiLayer Thin Film software [18,19]. The layer thicknesses were searched for based on the minimization of a merit function *MF* evaluating the closeness of the actual spectral characteristics to the target ones:

Optics EXPRESS

$$MF^2 = \sum_{j=1}^{61}\left(\frac{R^{(s)}\left(\mathbf{X};\lambda_{1,j}\right)-100\%}{\Delta_{1,j}}\right)^2 + \sum_{j=1}^{96}\left(\frac{R^{(p)}\left(\mathbf{X};\lambda_{2,j}\right)-100\%}{\Delta_{2,j}}\right)^2 + \sum_{j=1}^{201}\left(\frac{T^{(p)}\left(\mathbf{X};\lambda_{3,j}\right)-100\%}{\Delta_{3,j}}\right)^2, \quad (1)$$

where $\{\lambda_{1,j}\},\{\lambda_{2,j}\},\{\lambda_{3,j}\}$ are evenly distributed wavelength points in the spectral ranges of interest 770-830 nm, 860-1050 nm, and 4000-8000 nm, respectively; $\mathbf{X}=\{d_1,...,d_m\}$ is a vector of layer thicknesses; m is the number of layers; $\{\Delta_{1,j}\},\{\Delta_{2,j}\},\{\Delta_{3,j}\}$ are design tolerances in the corresponding wavelength ranges; (s) and (p) denote s- and p-polarization, respectively, angle of incidence is 67.9°. Varying tolerances allows one to strengthen or relax the corresponding target requirements. The target specifications are shown in Fig. 2 and Fig. 5 by crosses.

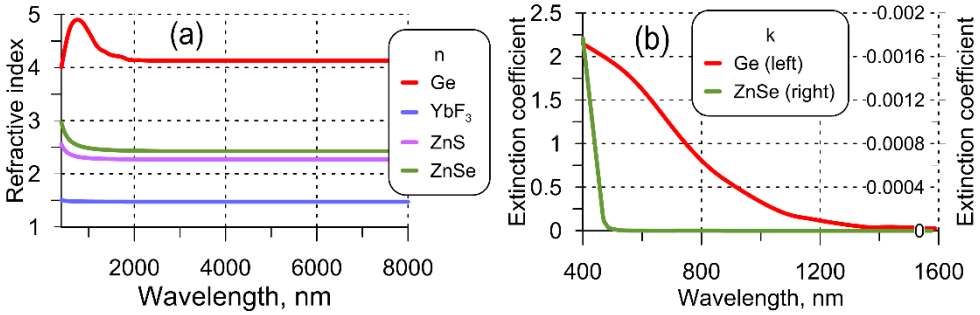

Fig. 1. (a) Refractive indices of thin-film materials and ZnSe substrate; (b) Extinction coefficients of Ge (left axis) and ZnSe substrate (right axis).

2.1 Beamsplitter comprising layers of YbF_3 and ZnS materials

First, a thin-film materials pair ZnS/YbF_3 was utilized for design. In the course of the design process, (1) different starting designs were used and (2) the tolerances (Eq. (1)) were varied. As the result, the optimal solutions were found to be in a vicinity of a pivotal 14-layer BS design (further *BS-ZnS/YbF*$_3$) with the profile shown in Fig. 3(a). It shows that the pattern of the profile resembles the structure of a quarter-wave mirror (QWM). In Fig. 2(a) and 2(c), reflectance in p- and s- polarization cases and transmittance (p-polarization) of the design are shown. For the sake of convenience, reflectance of the 14-layer QWM with the central wavelength of 920 nm and matching AOI of 67.9°is shown in Fig. 2(a).

The average reflectance/transmittance R_{av}/T_{av} and r.m.s deviations σ_R,σ_T were calculated with the 1 nm step in the HR and high transmittance (HT) zones for the p-polarization case:

$$R_{av} = \frac{1}{141}\sum_{j=1}^{141}R^p\left(860+j\right),\ T_{av} = \frac{1}{4001}\sum_{j=1}^{4001}T^p\left(4000+j\right),$$
$$\sigma_R = \sqrt{\frac{1}{141}\sum_{j=1}^{141}\left[R^p\left(860+j\right)-R_{av}\right]^2},\ \sigma_T = \sqrt{\frac{1}{4001}\sum_{j=1}^{4001}\left[T^p\left(4000+j\right)-T_{av}\right]^2} \quad (2)$$

Actually, smaller values of $\sigma_{T,R}$ indicate flatter spectral curves in the corresponding HR/HT spectral ranges.

It is seen from Fig. 2(a) that the p-polarized reflectance in the range 860-1050 nm does not reach high values and deviates significantly from the average reflectance value in this

Optics EXPRESS

range. Achieving high reflectance values (p-polarization) in the entire HR spectral range of interest at the large AOI of 67.9° is a critical point of the considered design problem. In other words, R_{av} should be as large as possible and σ_R (Eq. (2)) is to be as small as possible. The corresponding R_{av} and σ_R values are presented in Table 1. It is well-known that spectral performance of the multilayer can be improved on the expense of increase of the total thickness and the number of layers [20,21]. Increasing the thickness and correspondingly the number of layers with the help of the gradual evolution algorithm [20], one can obtain solutions with higher R_{av} values. The structure of all design solutions resembles the quarter-wave stacks as well. For example, in Fig. 2(b), spectral characteristics of a 20-layer beamsplitter (*BS-ZnS/YbF$_3$-20layers*) are presented. It is seen that although the p-polarized reflectance increases, it still cannot cover the entire spectral range 860-1050 nm (corresponding R_{av} and σ_R values are shown in Table 1). In addition to this, p-polarized transmittance in the MIR range 4-8 μm deviates significantly from the constant value. The structure of the 20-layer solution resembling a quarter-wave stack is shown in Fig. 3(b). For the sake of convenience, in Fig. 2(b), spectral characteristics of the corresponding 20-layer quarter-wave stack at the central wavelength of 920 nm are plotted. The similarity of the patterns of BS solutions and quarter-wave stacks allows one to provide rough analytical estimations explaining the impossibility to achieve high p-polarized reflectance values in the broadband spectral range at large AOI, i.e., to obtain a design with high R_{av} and low σ_R values. Actually, the reflectance $R^{(s,p)}(\lambda_0)$ at the central wavelength and the width of the HR zones $\Delta HR^{(s,p)}$ can be estimated using equations from [22], p. 74 and p. 77 rewritten for the oblique incidence case:

$$R^{(s,p)}(\lambda_0) \approx 1 - 4\frac{q_a^{(s,p)}}{q_s^{(s,p)}}\left(\frac{q_L^{(s,p)}}{q_H^{(s,p)}}\right)^m, \quad \Delta HR^{(s,p)} = \lambda_u^{(s,p)} - \lambda_d^{(s,p)},$$
$$\lambda_u^{(s,p)} = \lambda_0 \frac{\pi}{\pi - \arccos(-\xi^{(s,p)})}, \quad \lambda_d^{(s,p)} = \lambda_0 \frac{\pi}{\pi + \arccos(-\xi^{(s,p)})}, \tag{3}$$

where

$$\xi^{(s,p)} = \frac{\left(q_L^{(s,p)}\right)^2 + \left(q_H^{(s,p)}\right)^2 - 6q_L^{(s,p)}q_H^{(s,p)}}{\left(q_L^{(s,p)} + q_H^{(s,p)}\right)^2},$$
$$q_{L,H,s,a}^{(s)} = \sqrt{n_{L,H,s,a}^2 - n_a^2 \sin^2\theta}, \quad q_{L,H,s,a}^{(p)} = \frac{n_{L,H,s,a}^2}{\sqrt{n_{L,H,s,a}^2 - n_a^2 \sin^2\theta}} \tag{4}$$

In Eqs. (3), (4), n_H, n_L, n_s, n_a are refractive indices of ZnS, YbF_3, ZnSe, and air, respectively, θ is the AOI. The estimations of the maximum reflectance and widths of HR zones of the 14-layer and 20-layer stacks are calculated with the help of Eqs. (3), (4) and collected in Table 1. One can observe a remarkable agreement between these estimations and the corresponding values of the *BS-ZnS/YbF$_3$* and *BS-ZnS/YbF$_3$-20layers* design solutions. It follows from Eqs. (3), (4) that further increasing the number of layers and total coating thickness will lead only to an insignificant growth of the maximum p-polarized reflectance $R^{(p)}(\lambda_0)$ and as a consequence to an insignificant increase of R_{av}. The width of the HR zone does not depend on the number of layers and the coating thickness. It means that for the considered pair of thin-film materials, it is not possible to cover entirely a HR range broader than 160 nm. It should also be noted that further increase of the number of layers may lead to accumulation of

Optics EXPRESS

deposition errors and therefore to worsening of the produced sample performance. In addition to this, thicker coatings may exhibit larger stresses and cause adhesion problems. This issue is considered in detail in Section 3. In this case, a compromise between target specifications and feasibility demands has to be found since exploitation of ZnS/YbF_3 pair has limitations originated from physics. It should be noted that the spectral characteristics of the *BS-ZnS/YbF_3* design vary quite insignificantly in the angular range from 65 to 69°. This positive feature can be helpful in the course of implementation in laser setups. Taking into account all considerations listed above, a trade-off solution *BS-ZnS/YbF_3* was chosen for the deposition.

2.2 Beamsplitter comprising layers of YbF_3 and Ge materials

Similar to the case of ZnS and YbF_3 materials, multiple design attempts with another combination of thin-film materials, Ge and YbF_3, were undertaken. These attempts lead to quasi-periodic structures (QPS) of the type $\left[(2-p)L\middle|pH\right]^{m/2}$, with $p\approx 0.7$, L and H denote quarter-wave optical thicknesses of YbF_3 and Ge layers at the central wavelength of λ_0. Such structures have been carefully studied in [23], where analytical estimations of the achievable reflectance in the HR zone and the widths of the HR zones were obtained. Two design solutions containing 8 and 14 layers, denoted as *BS-Ge/YbF_3* and *BS-Ge/YbF_3-14layers*, are shown in Fig. 4. In Fig. 5, spectral characteristics of the design solutions and corresponding QPS comprising 8 and 14 layers are plotted. It is seen that the spectral performances of the design solutions and corresponding QPS are quite close.

The widths of the HR zones can be estimated using formulas from [23] rewritten for the oblique incidence case:

$$\Delta HR^{(s,p)}=\frac{4\lambda_0}{\pi}\frac{\sqrt{C^2-1}\sin(\pi p/2)}{C+1-(1-p^2)(C-1)\cos(\pi p)},\quad C=\frac{1}{2}\left(\frac{q_H^{(s,p)}}{q_L^{(s,p)}}+\frac{q_L^{(s,p)}}{q_H^{(s,p)}}\right),\qquad(5)$$

where $q_{H,L}^{(s,p)}$ are defined in Eq. (4), n_H, n_L are refractive indices of Ge and YbF_3, respectively.

Similarity to the case of the quarter-wave mirrors (Subsection 2.1), the width of the HR zone of the QPS depends on the ratios of high and low refractive indices only. It is seen in Fig. 5(a) that the reflectance covers its HR zone even when $m=8$. Due to the high ratio of the Ge and YbF_3 refractive indices, the HR zone is very broad even for p-polarized light at Brewster AOI. On the contrary to the ZnS/YbF_3 designs considered in Subsection 2.1, the bottle neck of the Ge/YbF_3 designs is the maximal achievable reflectance in both p- and s-polarization cases. The reason is that Ge films are absorbing up to 1200 nm and less absorbing in the range 1200-1900 nm. In addition, the optical constants of Ge films exhibit sophisticated patterns, see Fig. 1. Estimations performed with formulas published in [23] show that in the case of neglecting absorption in Ge layers, the reflectance in the HR zone could achieve a high level of 99.9% even for 8-layer solution. In the reality, presence of absorption in Ge layers reduces the achievable reflectance values down to the level of 75-80%. A rough analytical estimation of the decreased reflectance $R_{abs}^{(s,p)}$ can be obtained using expressions for the reflectance of a quarter-wave mirror in the absorbing case [22], p. 82:

$$R_{abs}^{(s,p)}\approx R^{(s,p)}(\lambda_0)-\frac{2\pi q_a^{(s,p)}k_H^{(s,p)}}{\left(q_H^{(s,p)}\right)^2-\left(q_L^{(s,p)}\right)^2},\qquad(6)$$

where k_H is the extinction coefficient of Ge film at the central wavelength λ_0.

Optics EXPRESS

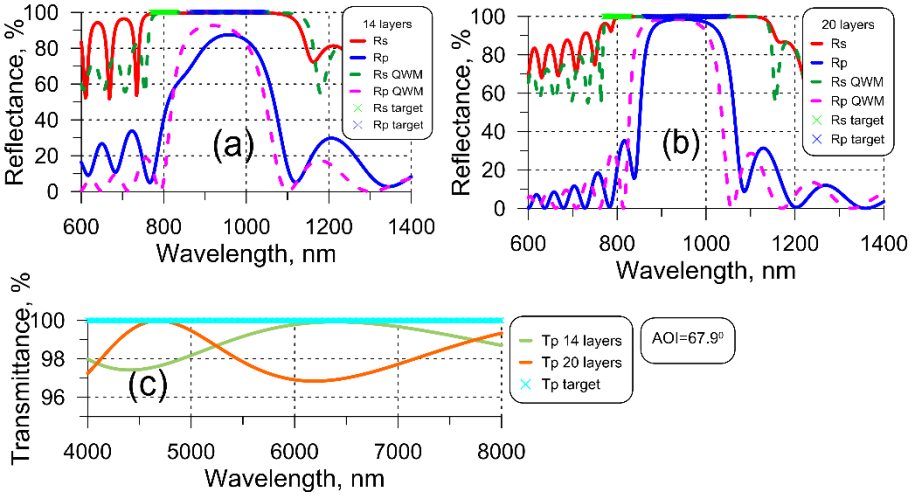

Fig. 2. Target and design reflectance of 14-layer (a) and 20-layer (b) BS-ZnS/YbF_3 solutions. Dashed lines plot corresponding spectral characteristics of the 14-layer and 20-layer QWM. (c) Target and design transmittance of 14-layer and 20-layer BS-ZnS/YbF_3 solutions.

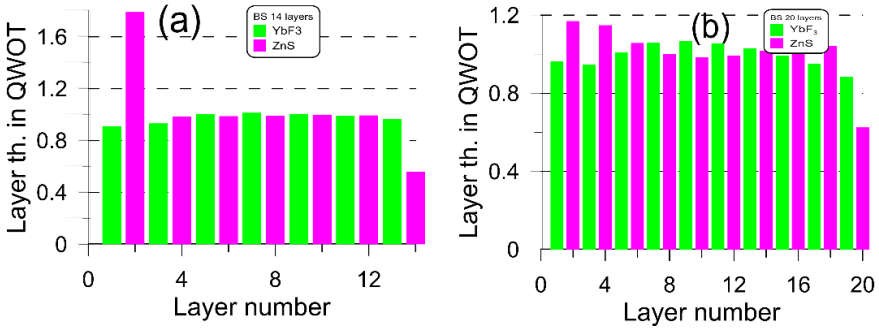

Fig. 3. Structures of the 14-layer (a) and 20-layer (b) BS-YbF3/ZnS solutions. Optical thicknesses of the layers are presented in QWOT at the wavelength of 920 nm and AOI = 67.9°.

Table 1. Characteristics of BS-ZnS/YbF_3 solutions and corresponding quarter-wave stacks, $\lambda_0 = 920nm$, $\Delta HR^{(s,p)}$ denotes the width of the HR zone.

Design/ Characteristic	$R^{(s)}(\lambda_0)$	$R^{(p)}(\lambda_0)$	$\Delta HR^{(s)}$	$\Delta HR^{(p)}$	R_{av}	σ_R	T_{av}	σ_T
BS-ZnS/YbF_3	99.0%	87.5%	335nm	160nm	81.2%	6.3%	99.0%	0.9%
QWM-ZnS/YbF_3-14layers	99.9%	92.0%	369nm	165nm	84.4%	11.6%	98.6%	1.4%
BS-ZnS/YbF_3-20layers	99.99%	98.5%	335nm	160nm	94.7%	5.6%	98.2%	1.0%
QWM-ZnS/YbF_3-20layers	99.999%	98.6%	369nm	165nm	88.1%	20.6%	97.8%	1.3%

In Table 2, the values of maximum reflectance of the 8-layer and 14-layer design solutions as well as estimations $R_{abs}^{(s,p)}$ calculated by (Eq. (6)) are presented. A good correspondence between predicted $R_{abs}^{(s,p)}$ and theoretical $R^{(s,p)}(\lambda_0)$ values of the design solutions is demonstrated. It is seen that increasing the number of layers and the coating thickness do not bring any improvements to the design performance. The spectral

Optics EXPRESS

characteristics of the *BS-Ge/YbF$_3$* design are almost insensitive in the angular range from 65 to 69° that is an important feature for implementing the optical element into laser setups. Due to this reason, the 8-layer solution BS-Ge/YbF$_3$ was chosen for the deposition.

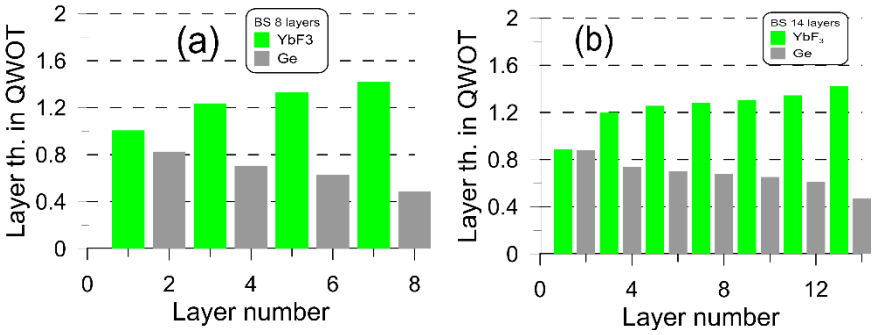

Fig. 4. Structures of the 8-layer (a) and 14-layer (b) BS-Ge/YbF$_3$ solutions. Optical thicknesses of the layers are presented in QWOT at the wavelength of 1000 nm and AOI = 67.9°.

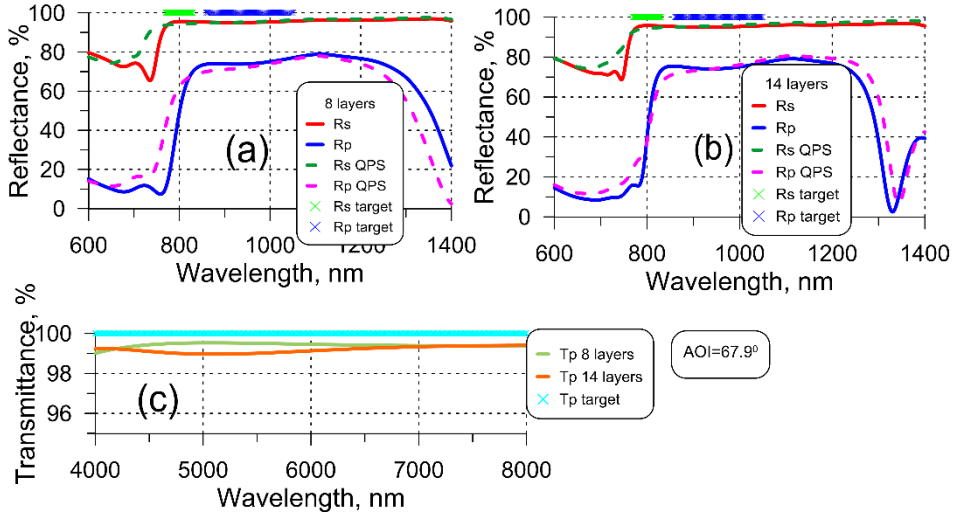

Fig. 5. Target and design reflectance of the 8-layer (a) and 14-layer (b) BS-Ge/YbF$_3$ solutions. Dashed lines plot the corresponding spectral characteristics of the 8-layer and 14-layer QPS. (c) Target and design transmittance of 8-layer and 14-layer BS-Ge/YbF$_3$ solutions.

2.3 Beamsplitter comprising layers of ZnS and Ge materials

Synthesis process based on the well established thin-film materials pair Ge/ZnS provides designs which are beneficial in comparison with neither Ge/YbF$_3$ nor ZnS/YbF$_3$ solutions found above. Multiple design attempts lead to QPS of the type $\left[(2-p)L\middle|pH\right]^{m/2}$, with $p \approx 0.6$, L and H denote quarter-wave thicknesses of ZnS and Ge layers at the central wavelength of λ_0, respectively. Spectral characteristics of a 14-layer *BS-Ge/ZnS* solution and the corresponding QPS are shown in Fig. 6(a). In Fig. 6(b), the structure of the *BS-Ge/ZnS* design is depicted. Increasing the number of design layers and coating thickness do not lead to improvement of the spectral performance. As Ge layers are absorbing, the average reflectance values in the HR zones do not exceed 91.5% and 69.8% in the case of s- and p-polarization, respectively. As the refractive index ratio of Ge and ZnS is not big in comparison to the pair Ge/YbF$_3$, the HR zones of *BS-Ge/ZnS* are narrower. These

Optics EXPRESS

considerations enable one to conclude that the Ge/ZnS pair is not suitable for the considered design problem.

It should be noted that both beamsplitters chosen for the deposition.

3. Production and characterization

Two experimental samples, named *BS-ZnS/YbF$_3$* and *BS-Ge/YbF$_3$*, were produced at the SyrusPro 710 high vacuum system (Leybold Optics GmbH, Alzenau, Germany). The samples are based on the corresponding designs *BS-ZnS/YbF$_3$* and *BS-Ge/YbF$_3$* discussed in Section 2. The coatings were deposited on ZnSe substrates of 1 mm thickness. The substrate temperature during the deposition was 120°. The vacuum system was pumped down to 10^{-6} mbar before the process. The deposition rates for Ge, ZnS, and YbF_3, were 0.6 nm/sec, 1 nm/sec, and 0.3 nm/sec, respectively. The evaporation materials Ge and YbF_3 were initially in granules of 0.7-3.5 mm, purity 99.999% and 1-3 mm, purity 99.99%, respectively. The materials were preconditioned in order to obtain solid discs. ZnS was in granules 1-5 mm, purity 99.99%. After the deposition, optical and mechanical properties of the samples were investigated.

- Adhesion testing is very important to evaluate the quality of optical coatings and their principal applicability in desired applications. A comprehensive review of different adhesion measurement techniques can be found in [24]. In the present work, a simplest type of adhesion test, a tape test, was used. According to [15], tape tests are addressed as test of "go-no-go" nature. A fresh piece of a kapton tape (1x1 cm) was carefully glued on the coating and then the tape was removed steadily in the direction normal to the coated surface. The tests were performed three time within half a year, every two months. Both samples exhibit excellent adhesion.

- Among a variety of environmental factors, which should be tested [15], the two that are important for potential applications of the produced filters in the laser setups, namely humidity and temperature influence. The samples were stored at room temperature without any special precautions. Their spectral characteristics, reflectance and transmittance, in the visible-near-infrared and mid-infrared ranges were recorded every two months. No shifts of the spectral curves were observed. The shift could be an evidence of increasing content of water in the samples. The thermal stability is important for laser related coatings [25]. The produced coatings can definitely survive at the temperatures up to 120-150°. Data on the laser damage threshold and thermal lensing lies out of the scope of the present study. The coatings will be implemented into laser setups and will not suffer from such environmental factors as corrosive fluids, rain, fog, dust storms, and vibrations.

- Normal incidence transmittance in the visible-near-infrared spectral range from 400 to 2600 nm was measured with the help of Lambda 950 spectrophotometer (Perkin Elmer) with the wavelength step of 2 nm. Excellent agreement between experimental and theoretical data can be observed in Fig. 7(a) and Fig. 9(a).

- Normal incidence transmittance data in the MIR range Fig. 8(a)-8(b) was recorded using Fourier transform infrared spectrometer Vertex 70 (Bruker Optics GmbH) several minutes after exposition of the samples from the deposition camera to the atmosphere and after 6 months (storage at room temperature, without any special precautions). It is seen that Ge/YbF_3 sample exhibits O-H absorption around 3 and 6 μm. On the contrary, there are no indications of O-H absorption in ZnS/YbF_3 filter. It should be noted that the films produced by e-beam evaporation do not exhibit ideal dense structure, porosity in the films is inevitable. After taking out to the atmosphere, the porous are filled with water that is clearly observed in Fig. 8. An absorption peak around 4.2 μm is presented in the measurement of the uncoated ZnSe substrate as well and can be attributed to water vapor in the air. The

Optics EXPRESS

outstanding feature of the produced samples is that they do not absorb additional O-H after a lapse period, see Fig. 8.

Table 2. Characteristics of the BS-Ge/YbF_3 solutions and corresponding quasi-periodic structures, $\lambda_0 = 1000\text{nm}$, $\Delta\text{HR}^{(s,p)}$ denotes the width of the HR zone.

Design/ Characteristic	$R_{abs}^{(s)}(\lambda_0)$		$R_{abs}^{(p)}(\lambda_0)$	$\Delta\text{HR}^{(s)}$	$\Delta\text{HR}^{(p)}$	R_{av}	σ_R	T_{av}	σ_T
BS-Ge/YbF_3	95.4%		75.1%	650nm	490nm	74.6%	0.9%	98.5%	0.3%
QPS-Ge/YbF_3-8layers	96.3%		74.5%	683nm	500nm	73.7%	1.8%	99.0%	0.3%
BS-Ge/YbF_3-14layers	95.3%		75.0%	650nm	490nm	74.9%	0.8%	99.2%	0.2%
QPS-Ge/YbF_3-14layers	96.3%		74.5%	683nm	500nm	74.7%	1.7%	98.9%	0.8%

- Quasi-normal incidence reflectance as well as oblique incidence reflectance in s- and p-polarization cases at AOI = 45° was measured at the Universal Reflectance Accessory of Lambda 950 in the spectral range of 400-2200 nm, Fig. 7(c) and Fig. 9(c).
- Reflectance at the Brewster angle of 67.9° was measured using a Universal Measurement Accessory of the Cary 7000 spectrophotometer in a spectral range of 400-2500 nm. In Fig. 7(d) and Fig. 9(d), an excellent correspondence between experimental and theoretical spectral performances can be observed.
- Mechanical stresses of the samples were estimated using the formula from [5,6]:

$$\sigma_M = \frac{\Sigma_H \sigma_H + \Sigma_L \sigma_L}{\Sigma_M}, \tag{7}$$

where σ_M is the stress in the coating, $\Sigma_H, \Sigma_L, \Sigma_M$ are geometrical thicknesses of high-, low-index layers, and total thickness of the coating, respectively, σ_H, σ_L are stresses in high- and low-index layers, respectively. Stresses in separate materials σ were determined based on the well-known Stoney formula [5,26]:

$$\sigma = \frac{1}{6}\left(\frac{1}{R_2} - \frac{1}{R_1}\right)\frac{E \cdot \Sigma_s^2}{(1-\nu)\Sigma_f}, \tag{8}$$

where E and ν are Young's modulus and Poisson's ratio of the substrate, respectively, Σ_s and Σ_f are thicknesses of the substrate and a single thin film, R_1, R_2 are radius of curvature before and after deposition, respectively. First, the radius of curvature R_1 of several 1-mm glass substrates were measured using Dektak 150 Stylus Profiler (Veeco). Then, thick layers of Ge, ZnS, and YbF_3 were deposited on these pre-measured substrates, and the radius R_2 were measured at the Profiler. Stress values of Ge, ZnS, and YbF_3 were calculated using Eq. (8) equal to (−50) MPa, (−400) MPa, and 140 MPa, respectively. It means that Ge and ZnS layers exhibit compressive stress, and YbF_3 films have tensile stress [14].

Geometrical thicknesses of high- and low-index layers and stresses in the designed coatings *BS-ZnS/YbF_3, BS-ZnS/YbF_3-20layers, BS-Ge/YbF_3,* and *BS-Ge/YbF_3-14layers* are collected in Table 3. It is seen that the total stresses are not big since the stresses in high- and low-index materials compensate each other. It can be also observed in Table 3 that absolute

Optics EXPRESS

values of stresses in ZnS/YbF_3 and Ge/YbF_3 coatings are comparable. In the last row of Table 3, expected values of the stress in the beamsplitter comprising ZnS and Ge layers (Section 2.3) is presented. One can see that these values are higher than the stresses in the ZnS/YbF_3 and Ge/YbF_3 beamsplitters.

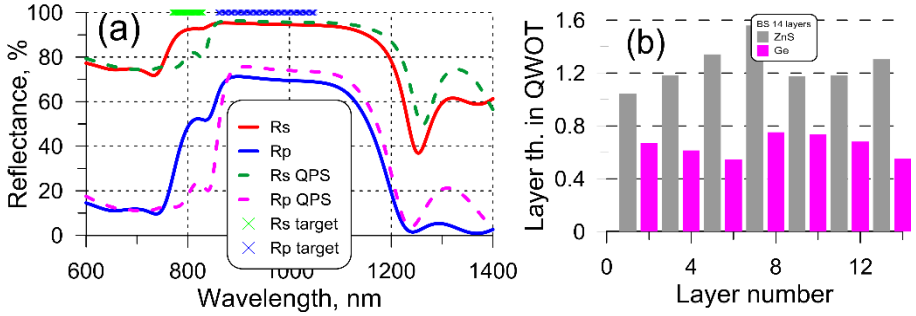

Fig. 6. (a) Target and design reflectance of the 14-layer BS-Ge/ZnS solution. Dashed lines plot corresponding spectral characteristics of the 14-layer QPS. (b) Structures of the 14-layer BS-Ge/ZnS solution. Optical thicknesses of layers are calculated at the wavelength of 1000 nm.

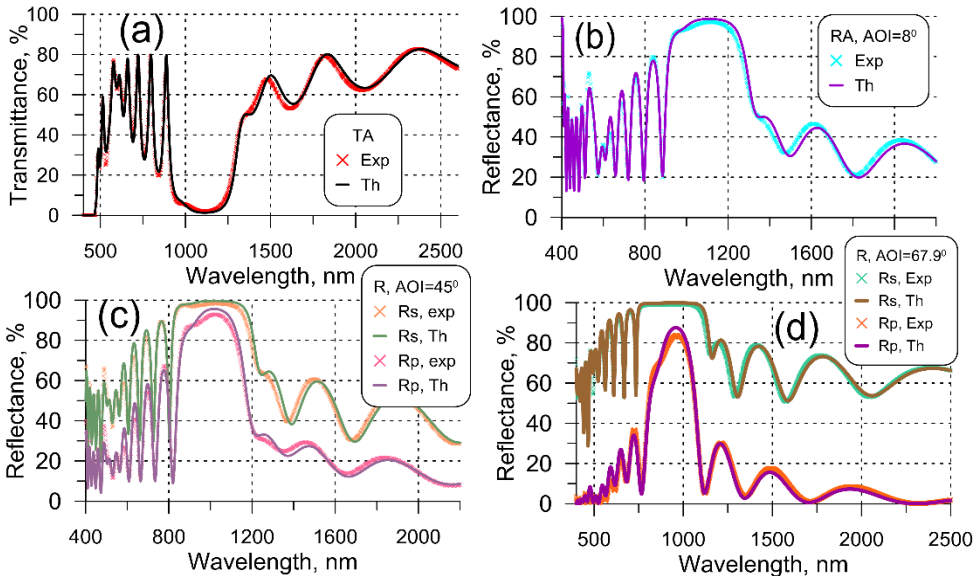

Fig. 7. Comparison of theoretical and experimental spectral characteristics of the produced BS-ZnS/YbF_3 sample: (a) transmittance measured in the visible-near-infrared range, (b) quasi-normal incidence reflectance (average polarization), (c) s- and p-polarized reflectance at the AOI = 45°, (d) reflectance at the Brewster AOI = 67.9°. The measurements at the Brewster angle were performed at Agilent technologies.

Table 3. Stresses in designed coatings, experimental designs are marked by bold.

Design	Σ, nm	Σ_{YbF_3}, nm	Σ_{Ge}, nm	Σ_{ZnS}, nm	σ_M, GPa
BS-ZnS/YbF$_3$	2162	1364		798	–60 MPa
BS-ZnS/YbF_3-20layers	3093	1992		1101	–52 MPa
BS-Ge/YbF$_3$	1231	1086	145		118 MPa
BS-Ge/YbF_3-14layers	2152	1893	259		118 MPa
BS-Ge/ZnS-14 layers	1295		249	1047	–330 MPa

Optics EXPRESS

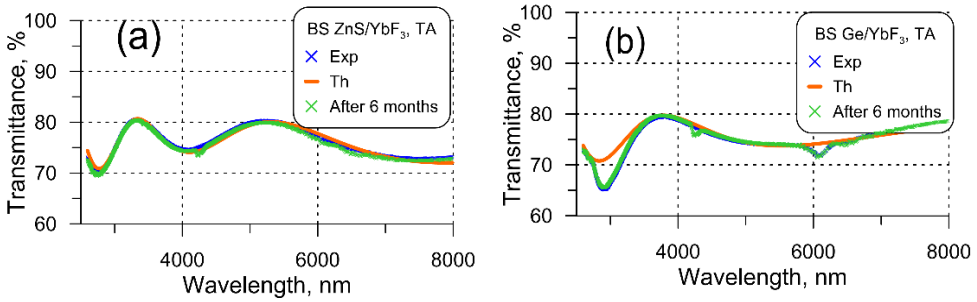

Fig. 8. Comparison of the theoretical and experimental transmittance in the MIR spectral range of the produced BS-ZnS/YbF_3 (a) and BS-Ge/YbF_3 (b) samples. The experimental transmittance was recorded several minutes after exposure to the atmosphere and 6 months later.

4. Discussion

The study carried out in the present work demonstrates two pairs of materials suitable for the production of sophisticated broadband coatings operating in the near-infrared and mid-infrared spectral ranges. Two beamsplitters consisting of ZnS/YbF_3 and Ge/YbF_3 layers were designed, produced and characterized. The beamsplitters operate at the Brewster angle of the ZnSe substrate. Excellent agreement between experimental and theoretical curves of the produced samples confirms the reliability of the dispersion curves of all three thin film materials and ZnSe substrate. Measurements of mechanical stresses show that due to opposite signs of the deflections caused by high- and low-index layers, the total stresses of the produced multilayers are at a quite low level. In Table 4, *pro et contra* of ZnS/YbF_3 and Ge/YbF_3 combinations are collected.

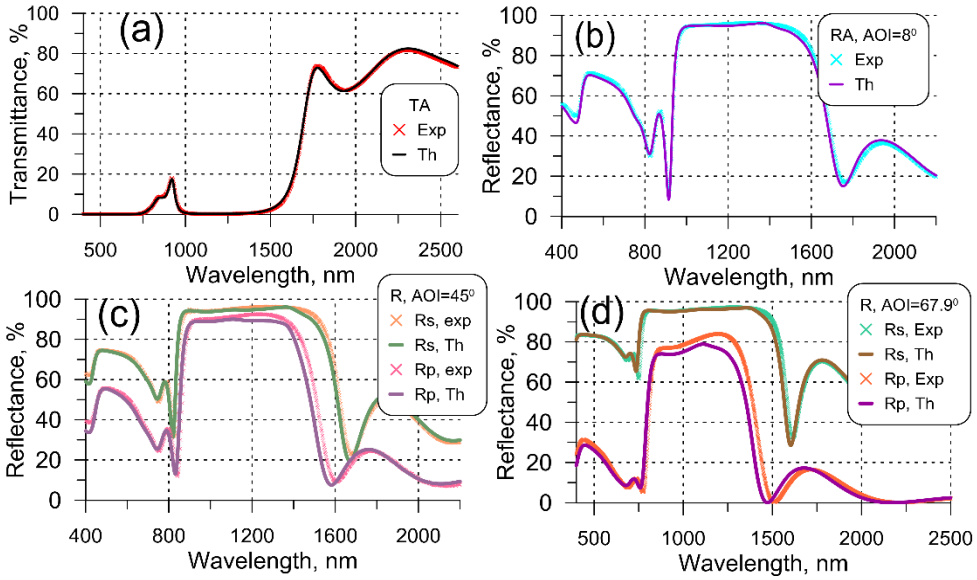

Fig. 9. Comparison of theoretical and experimental spectral characteristics of the produced BS-Ge/YbF_3 sample: (a) transmittance measured in the visible-near-infrared range, (b) quasi-normal incidence reflectance (average polarization), (c) s- and p-polarized reflectance at the AOI = 45°, (d) reflectance at the Brewster angle of 67.9°. The measurements at the Brewster angle were performed at Agilent technologies.

Optics EXPRESS

Table 4. Qualitative comparison of beamsplitters comprising ZnS/YbF_3 and Ge/YbF_3 pairs

Characteristic	ZnS/YbF_3	Ge/YbF_3
R_{av} in $HR^{(s)}$ zone	higher	lower
R_{av} in $HR^{(p)}$ zone	higher	lower
Flatness in $HR^{(s)}$ zone	the same	the same
Flatness in $HR^{(p)}$ zone	lower	higher
Flatness in $HT^{(p)}$ zone	lower	higher
Number of layers	larger	smaller
Total thickness	larger	smaller
Stresses	comparable	comparable

5. Conclusions

The estimations presented in Section 2 of the present work demonstrate that the only one disadvantage of the Ge/YbF_3 multilayers in comparison with ZnS/YbF_3 coatings is that Ge layers are increasingly absorbing in the considered spectral range from 770 to 1050 nm since this is the range of the dominance of electronic transitions [27]. However, due to a big refractive index ratio of Ge and YbF_3 thin-film materials, even this absorption is not essential limiting factor. Evidently, moving to the longer wavelengths, absorptance in Ge layers will decrease rapidly and therefore, Ge/YbF_3 pair has a very large potential for design and production of NIR-MIR coatings.

Funding

The DFG Cluster of Excellence, "Munich Centre for Advanced Photonics," (http://www.munich-photonics.de.

Acknowledgments

The authors thank Agilent Technologies for performing the reflectance measurements.

References

1. M. J. Baker, J. Trevisan, P. Bassan, R. Bhargava, H. J. Butler, K. M. Dorling, P. R. Fielden, S. W. Fogarty, N. J. Fullwood, K. A. Heys, C. Hughes, P. Lasch, P. L. Martin-Hirsch, B. Obinaju, G. D. Sockalingum, J. Sulé-Suso, R. J. Strong, M. J. Walsh, B. R. Wood, P. Gardner, and F. L. Martin, "Using Fourier transform IR spectroscopy to analyze biological materials," Nat. Protoc. **9**(8), 1771–1791 (2014).
2. J. Hodgkinson and R. P. Tatam, "Optical gas sensing: a review," Meas. Sci. Technol. **24**(1), 012004 (2013).
3. M. Huber, W. Schweinberger, M. Trubetskov, S. A. Hussain, O. Pronin, L. Vamos, E. Fill, A. Apolonski, M. Zigman, F. Krausz, and I. Pupeza, "Detection sensitivity of field-resolved spectroscopy in the molecular fingerprint region," in *CLEO/Europe-EQEC* (2017), p. CH-P_4.
4. A. V. Muraviev, V. O. Smolski, Z. E. Loparo, and K. L. Vodopyanov, "Massively parallel sensing of trace molecules and their isotopologues with broadband subharmonic mid-infrared frequency combs," Nat. Photonics **12**(4), 209–214 (2018).
5. A. E. Ennos, "Stresses Developed in Optical Film Coatings," Appl. Opt. **5**(1), 51–61 (1966).
6. K. Hendrix, J. D. T. Kruschwitz, and J. Keck, "Optical Interference Coatings Design Contest 2013: angle-independent color mirror and shortwave infrared/midwave infrared dichroic beam splitter," Appl. Opt. **53**(4), A360–A376 (2014).
7. G. Wang, X. Ling, X. Liu, and Z. Fan, "Effects of deposition temperature on characterization and laser-induced damage threshold of YbF3 films," Opt. Laser Technol. **49**, 274–278 (2013).
8. W. Su, B. Li, D. Liu, and F. Zhang, "The determination of infrared optical constants of rare earth fluorides by classical Lorentz oscillator model," J. Phys. Appl. Phys. **40**(11), 3343–3347 (2007).
9. M. Kennedy, D. Ristau, and H. Niederwald, "Ion beam-assisted deposition of MgF2 and YbF3 films," Thin Solid Films **333**(1-2), 191–195 (1998).
10. M. Stolze, "Fluoride materials for high-quality IR coatings," in *Optical Interference Coatings* (OSA, 2010), p. ThA2.
11. UMICORE Materials AG, "Special materials for precision optics and laser coatings, Fluorides and special materials for IR coatings".
12. J. D. Traylor Kruschwitz and W. T. Pawlewicz, "Optical and durability properties of infrared transmitting thin films," Appl. Opt. **36**(10), 2157–2159 (1997).

Optics EXPRESS

13. Y. Wang, Y. G. Zhang, W. L. Chen, W. D. Shen, X. Liu, and P. F. Gu, "Optical properties and residual stress of YbF3 thin films deposited at different temperatures," Appl. Opt. **47**(13), C319–C323 (2008).
14. M. Friz and F. Waibel, "Coating materials," in *Optical Interference Coatings* (Springer, 2003), pp. 105–130.
15. H. A. Macleod, *Thin-Film Optical Filters*, 4th ed. (Taylor & Francis, 2010).
16. T. V. Amotchkina, V. Janicki, J. Sancho-Parramon, A. V. Tikhonravov, M. K. Trubetskov, and H. Zorc, "General approach to reliable characterization of thin metal films," Appl. Opt. **50**(10), 1453–1464 (2011).
17. T. V. Amotchkina, M. K. Trubetskov, A. V. Tikhonravov, V. Janicki, J. Sancho-Parramon, and H. Zorc, "Comparison of two techniques for reliable characterization of thin metal-dielectric films," Appl. Opt. **50**(33), 6189–6197 (2011).
18. A. V. Tikhonravov, M. K. Trubetskov, and G. W. Debell, "Application of the needle optimization technique to the design of optical coatings," Appl. Opt. **35**(28), 5493–5508 (1996).
19. M. Trubetskov and A. Tikhonravov, *OptiLayer Thin Film Software* (n.d.).
20. A. V. Tikhonravov, M. K. Trubetskov, T. V. Amotchkina, and M. A. Kokarev, "Key role of the coating total optical thickness in solving design problems," SPIE Proc. **5250**, 312–321 (2004).
21. A. Thelen, M. Tilsch, A. V. Tikhonravov, M. K. Trubetskov, and U. Brauneck, "Topical Meeting on Optical Interference Coatings (OIC '2001): design contest results," ao **41**, 3022–3038 (2002).
22. S. A. Furman and A. V. Tikhonravov, *Basics of Optics of Multilayer Systems* (Editions Frontières, 1992).
23. T. V. Amotchkina, "Analytical estimations for the reference wavelength reflectance and width of high reflection zone of two-material periodic multilayers," Appl. Opt. **52**(19), 4590–4595 (2013).
24. K. L. Mittal, "Adhesion Measurement of Thin Films," Electrocompon. Sci. Technol. **3**(1), 21–42 (1976).
25. T. Amotchkina, M. Trubetskov, and V. Pervak, "Experimental and numerical study of the nonlinear response of optical multilayers," Opt. Express **25**(11), 12675–12688 (2017).
26. S. Kičas, U. Gimževskis, and S. Melnikas, "Post deposition annealing of IBS mixture coatings for compensation of film induced stress," Opt. Mater. Express **6**(7), 2236 (2016).
27. E. Palik, *Handbook of Optical Constants of Solids II* (Academic, 1991).